Resistive hydrogen sensing response of Pd-decorated ZnO "nanosponge" film

Meng Zhao[a]*, Man Hon Wong[b], Hau Chung Man[c], and Chung Wo Ong[b]*

[a]   Research Center for Solid State Physics and Materials, School of Mathematics and Physics, Suzhou University of Science and Technology, Suzhou 215009, P.R. China

[b]   Department of Applied Physics and Materials Research Center, The Hong Kong Polytechnic University, Hung Hom, Kowloon, Hong Kong, P.R. China

[c]   Department of Industrial and Systems Engineering, The Hong Kong Polytechnic University, Hung Hom, Kowloon, Hong Kong, P.R. China

*   Author to whom correspondence should be addressed. E-mail: mzhao@usts.edu.cn and c.w.ong@polyu.edu.hk; Tel: (852) 2766 5689; Fax: (852) 2333 7629

1

ABSTRACT

Hydrogen (H_2)-induced resistive response of palladium (Pd)-decorated zinc oxide "nanosponge" (Pd/ns-ZnO) film was studied at different operation temperatures with and without UV illumination. The as-deposited ns-ZnO film, fabricated using a supersonic cluster beam deposition system, was highly porous and composed of ~5 nm nanoclusters embedded in an amorphous matrix. After annealed at 500 ^{o}C for 1 hr, the film was found to contain loosely connected 13 nm crystallites and had a porosity of 73 %. The Pd/ns-ZnO film sensor at 20 ^{o}C showed a sensor response of 82 and a response time of 1 s for 2 % H_2. After heated slightly to 80 ^{o}C, the sensor response was increased by 43 times, and the response and recovery times dropped to 0.3 s and 18 s, respectively. This performance is superior to those of many other metal oxide nanomaterials operating at temperatures > 200 ^{o}C. The sensing properties of the Pd/ns-ZnO film showed little degradation when UV illumination was applied, but the sensing stability was improved. A reaction model was proposed to give an explanation to the gas sensing process. The influences of increasing the operation temperature and UV illumination are discussed.

Keywords: H_2 sensor; ZnO film; high porosity; fast response; UV assisted gas detection

2

1. Introduction

As a clean and renewable energy source, hydrogen is considered to be an important part of future energy landscape [1,2]. Because H_2 is highly explosive, stringent standards of H_2 sensors used for monitoring H_2 leakage have been proposed by many governmental departments and professional bodies, like the US Department of Energy and manufacturers of H_2 powered vehicles [3-6]. In particular, new sensors are required to have a response time < 1 s, which is far beyond the capability of many existing commercialized H_2 sensor products [3]. A new trend is to further require new gas sensors to have low power consumption [5-7], such that they can be used to build up a large-scaled monitoring system like a wireless sensor network with individual sensor elements to be operated for a long time by being powered with small batteries. This means that other than having good sensing properties, the sensor is required to be workable at ambient temperature without needing a heater as in the case of a conventional metal oxide (MO_x) sensor which is required to be operated at an elevated temperature usually above 200 ^{o}C [8].

MO_x nanomaterial is considered to be a promising candidate for making new advanced H_2 sensors [9-14]. Based on the present consensus, MO_x nanomaterial suitable for gas sensor development should have (i) a large porosity to enlarge the contact area with the detected gas so as to enhance the sensor response and accelerate the reaction rate [15-20], and (ii) small crystallite size to achieve a large fractional volume change of the depletion layer compared to the nano grain size such that a large sensor response can be obtained [20-24]. These two features are often not achievable in a single nano-MO_x material according to the published research articles. For example, zero-dimensional MO_x nanoparticles with small crystallite size showed large sensor response even at room temperature [25,26], but the response time is long because the nanoparticles agglomerate to form a dense matrix in which the detected gas

3

species can only migrate slowly. Another example is that a one-dimensional MO_x nanomaterial provides a large surface for the reaction such that a fast response rate is achieved [27-29], but the output signal is relatively small because the particle size is relatively large compared to that of zero-dimensional nanoparticles. Therefore, how to make nano-MO_x gas sensing materials having both of high porosity and small average grain size becomes a challenging problem.

Supersonic cluster beam deposition (SCBD) is a powerful technique to be used for producing thin films composed of MO_x nanoclusters [30]. In this work, we attempted to use this technique to produce nanosponge-like zinc oxide (ns-ZnO) thin films. They are expected to have a highly porous structure composed of loosely packed genuine ZnO nanoclusters. This is an ideal structure to be pursued for gas sensing research. In addition, investigation on the influences of a slight increase in the operation temperature and UV assist on the hydrogen sensing properties of the film material is also a focus of the study. A reaction model is proposed to give qualitative explanation for the findings.

2. Experimental methods

ns-ZnO films were deposited using an SCBD system (Tethis, Italy) [30]. In an SCBD process, 1 % O_2-Ar gas was pulsed on a rotating Zn metal rod target at a frequency of 4 Hz. Electric pulses of -800 V were applied to the rod with a time lag of 220 μs to generate microplasma plumes. The ablated species from the Zn rod were oxidized in the oxygen-containing atmosphere and were condensed to become ZnO nanoclusters. They were then carried by the gas flow to enter an expansion chamber. After passing through a set of aerodynamic lens, the nanoclusters were aligned and collimated in a single direction. They finally entered a deposition chamber in high vacuum condition and were deposited on

Corning 7059 glass substrates and Si wafers. A film on Si wafer is suitable to be used for cross-section transmission electron microscope (TEM) analysis. The as-deposited films were annealed in an oxygen atmosphere at 500 ^{o}C for 1 hr using a rapid thermal annealing furnace to further stabilize the film structure. X-ray diffraction (XRD with Cu Kα source, Bruker D8 Advance), scanning electron microscope (SEM, Hitachi SU8010) and TEM (FEI, Tecnai G2F20) were used to characterize the film structure.

Fig.1 shows the structure of a film sample. A 5 nm palladium (Pd) layer was sputtered on top of the annealed ns-ZnO film to work as a catalyst layer. Pd is known to be capable of dissociating H_2 molecules into atoms so as to lower the energy barrier for subsequent surface reactions [19]. Two silver paste electrodes are made on the film surface. They are separated by a distance of 5 mm. The Pd/ns-ZnO film sensor thus produced was mounted in the test chamber of a homemade measurement system [31]. The structure and working principle of the system are shown in Fig. 2. The chambers, electromagnetic valves V1-V12 and pipeline form a vacuum compatible system. The automation of measurement process is realized using a LabVIEW program through an analog-to-digital (A/D) interfacing module (NI, Model USB-6343). In brief, the A/D module records the signals of two pressure sensors, a relative humidity (RH) sensor and thermocouple. The LabVIEW program compares the measured valves with the set points and generates control signals to operate the electromagnetic valves, heaters and the mass flow controllers (MFC). More details are reported in Ref. [31] and the supporting information document.

A normal test circle contains three steps. Step 1 – preparation of a sample gas: The mixing chamber (Fig. 2) is first evacuated by a vacuum pump. 2 % H_2-air admixture from a gas cylinder is then admitted into the mixing chamber via an MFC. The partial pressure of this gas is recorded by two absolute pressure sensors P1 and P2 calibrated to work at different

ranges. After reaching the target value p_{H_2}, synthetic air from another cylinder is then admitted into the mixing chamber for the total pressure p_{total} to reach 1.1 bar. The hydrogen concentration is equal to $p_{H_2}/p_{total}*2$ %. Step 2 – measurement of sensor response: The test chamber is evacuated by the vacuum pump. Valves V9 and V11 are then opened for the sample gas charged up in the mixing chamber to be released to the measurement chamber. Equilibrium is reached shortly, whereas the pressures in the two chambers (with a volume ratio of 10 to 1) are all equal to 1 bar. Step 3 – observation of recovery: The test chamber is evacuated by the vacuum pump and then filled with synthetic air by opening valves V1, V4, V8 and V11. These valves will close automatically when the chamber pressure reaches 1 bar. To our knowledge, quick gaseous exchange technique in gas sensing measurements is seldom applied, but the response and recovery times detected with this method are closer to the real ones, because the error due to the slower diffusion process can be diminished.

The relative humidity of the sample gas was controlled by the temperatures of water chamber (Fig. 2) and opening time of valves V3 and V4. The Pd/ns-ZnO film sensor was heated up by two cartridge heaters inserted in a stainless steel block, which also held the sample, test pins and thermocouple. Two settings of measurement temperature, i.e. 20 ^{o}C and 80 ^{o}C with an accuracy of 0.1 ^{o}C were used in the tests. The electrical resistance of the Pd/ns-ZnO film was measured using a Keithley 617 electrometer (input impedance $> 2\times10^{14}$ Ω). The methods used for noise suppression are summarized in the supporting information. Data were acquired and recorded using the LabVIEW software. To study the effect of ultraviolet (UV) illumination on the hydrogen sensing behaviors of Pd/ns-ZnO film sensor, a 365-nm light emitting diode (LED) was used to generate UV light to shine on the sample. The light intensity reaching the film surface was measured to be 10 mW/cm^{2}.

Three H_2 sensing performance indices were derived from the resistive response of the Pd/ns-ZnO film sample. They are the sensor response S, response time t_{res} and recovery time t_{rec}, respectively. S is defined as R_{air}/R_{H_2}, where R_{air} and R_{H_2} are saturated film resistance in air and H_2-air admixture respectively. t_{res} and t_{rec} are defined as the duration for the sensor's resistance to drop and recover by 90 % of the total resistance change, i.e. R_{air} -R_{H_2}.

3. Results and discussion

3.1 Structure of ns-ZnO film

The XRD spectrum of the as-deposited ns-ZnO film (Fig. 3) only shows the diffraction peaks associated with crystalline ZnO (JCPDS card, No. 36-1451), but no any sign from the Zn metal. This confirms that the film has already been well oxidized during deposition. The average crystallite size estimated from the XRD data using the Scherrer equation is ~5 nm. The presence of nano-sized clusters in the as-deposited film is clearly seen in the SEM image as shown in Fig. 4a. More importantly, the as-deposited ns-ZnO film is highly porous, with the presence of numerous pores of a few tens of nm in diameters. The porosity of an ns-ZnO film is $\theta = (1-z_{mass}/z_{real})\times100$ %, where z_{mass} is the mass equivalent thickness of ns-ZnO film measured with a quartz monitor during deposition (16.1 nm), and z_{real} is the real thickness measured by surface profiler (89.3 nm), which is estimated to be 82 % for an as-deposited film.

The as-deposited ns-ZnO film was annealed at 500 ^{o}C in O_2 for 1 hr aiming to stabilize the film structure. After annealing, the XRD spectrum shows much stronger and sharper diffraction peaks (Fig. 3). The calculated average crystallite size is ~13 nm. We propose that at the time when crystallites grow at the post-oxidation temperature, the film also shrinks concomitantly but mainly in the out-of-plain direction. The thickness z_{real} reduced from 89.3

to 59.9 nm, but the porosity remained as high as 73 %. Furthermore, the original pores were not eliminated by the heat treatment (see Fig. 4b). This feature is expected to facilitate fast diffusion of detected gas species in the film and favorable for the achievement of strong and fast sensor response.

The cross-section TEM image of the 500 ^{o}C post-oxidized ns-ZnO film as shown in Fig. 5a confirms that the film is composed of loosely connected nanoclusters with diameter in the range of 10-15 nm. Nano sized pores and voids are clearly seen in the intra-cluster regions. High resolution TEM image (Fig. 5b) further reveals the single-crystal structure of the annealed clusters. The lattice spacing is determined to be 0.258 nm, which is consistent with the d-spacing of (0002) lattice planes of hexagonal ZnO and agrees well with the XRD result. Now, we assert that the annealed ns-ZnO film is highly porous and composed of loosely connected 13-nm crystallites. Such a structure is expected to exhibit fast and strong resistive response to H_2 due to fast diffusion rate of the gas in the film and a large surface-to-volume ratio of the film structure.

3.2 Effect of operation temperature

We investigated the resistive response of the Pd/ns-ZnO film to 2 % H_2 in air at 20 ^{o}C, to examine how the nanosponge-like structure favors the realization of low-temperature gas detection. Results are shown in Fig. 6a. The resistance of the Pd/ns-ZnO film decreased from 3.41×10^9 Ω to 3.7×10^8 Ω in 1 s, and was quickly stabilized at ~4×10^7 Ω. After waiting for 15 s, the test ambient was switched to air. The film resistance was restored to its initial value in 70 s. The response and recovery time were determined to be 1 s and 52 s respectively. It should be noted that the response time of the Pd/ns-ZnO film is shorter than those of many other MO_x-based H_2 sensors operated at room-temperature, which is mostly in the range of

8

minutes [32-36]. The fast response rate of the ns-ZnO film at 20 ^{o}C leads us to assert that the highly porous structure makes the supersonic cluster beam deposited (SCBD) ns-ZnO to be an excellent candidate of gas sensing material in the applications requiring fast detection of a hazardous gas.

However, when operated at room temperature, the resistive response is easily affected by presence of water vapor and/or the temperature fluctuation. Therefore, the sensor should be heated up slightly in real applications to eliminate the effect of temperature and humidity variation. Fig 6b compares the resistive response of the Pd/ns-ZnO film to 2 % H_2 in air measured at 20 ^{o}C and 80 ^{o}C respectively. We first note that the base resistance R_{air} of the film measured at 80 ^{o}C is higher than that measured at 20 ^{o}C. Considering that the film sensor is composed of a metal Pd layer and a semiconducting ZnO layer, when temperature increases, the resistance of the Pd metal layer would increase due to stronger electron scattering and mild thermal stress-induced degradation of the continuity of the Pd layer. Though the semiconducting ZnO layer becomes more conducting concurrently, the former two factors prevail to result in a drop of the overall resistance of the bilayer structure. However, its influence is minor compared to that associated with the gas sensing effect (Table 1). In summary, (i) S increases from 82 to ~3540, corresponding to a 43 times increase compared to the one detected at 20 ^{o}C; (ii) t_{res} and t_{rec} decrease from 1 s and 52 s to 0.3 s and 18 s respectively, namely about 1/3 of the ones detected at 20 ^{o}C. The overall improvement of sensing performance at 80 ^{o}C can be attributed to the faster reaction rates of the chemical processes responsible for the gas sensing effect, which include dissociation of H_2 at Pd surface, diffusion and spilling over of H species to the ZnO layer, surface reaction between H and adsorbed O_2^{-}, and re-adsorption of O_2^{-}, etc.

Fig. 7 shows the effect of changing the relative humidity (RH) in the detected environment on the sensor's performance measured at 80 ^{o}C. As the RH value increased from 0 % to 50 %, the response curves are almost unchanged. When it was further increased to 90 %, the film resistance in air decreased slightly, but the resistance in the presence of hydrogen still remained unchanged. This is because that at this temperature physisorbed H_2O molecules are basically removed [37,38], while chemisorbed H_2O molecules are not present yet [39]. As such the sensor appears to be insensitive to the water vapor contained in the detected area. Furthermore, compared to room temperature, a slightly elevated operation temperature of 80 ^{o}C helps to stabilize the sensor's output signal against the influence of ambient temperature fluctuation.

We further compare the H_2 sensing performance of the Pd/ns-ZnO film with those of other nano MO_x-based materials reported in literatures. Fig. 8 shows the resistive response of the Pd/ns-ZnO film to H_2 measured in air at 80 ^{o}C, with the H_2 concentration varying in the range of 0.1–2 %. The sensor response and response rate were found to increase with increasing H_2 concentration. The values of S and t_{res} derived from the data are plotted in Fig. 9 as functions of H_2 concentration. The published data for zero-dimensional [40-44] and one-dimensional [45-47] MO_x nanomaterials are labeled with solid and hollow symbols respectively, where all of them are claimed to be obtained from measurements conducted at temperatures > 200 ^{o}C. Note that the published data falling in the shaded area are interior to that of ours (either smaller S or longer t_{res}), that those lying outside are superior to ours. Comparison shows that S of our Pd/ns-ZnO film is higher than most of these reported results in the H_2 concentration range of 0.1–2 %. Exceptions are the Pt activated $TiO_2:WO_3$ nanocrystalline film working at 200 ^{o}C [40] and Pd activated WO_3 nanocrystalline film working at 350 ^{o}C [41], which exhibit larger S values. However, their t_{res} values are at least 5

times longer than our present result. One also sees that t_{res} of the Pd/ns-ZnO film is shorter than most reported values of the materials working at temperatures > 200 ^{o}C. Exceptions are the carbon nanotube and tin oxide nanoparticles hybrid thin film (CNT-SnO$_2$) working at 250 ^{o}C [42] and SnO$_2$ nanofibers working at 320 ^{o}C [46], which have shorter t_{res}, but their S values are about 1/10 to 1/3 of our sample. The superiority of the H$_2$ sensing properties of Pd/ns-ZnO film is thus confirmed.

3.3 Effect of UV irradiation and the reaction model

It is often reported that the use of UV illumination can enhance the gas sensing performance of a nanoclustered direct band-gap semiconductor metal oxide, e.g. ZnO [48-51], SnO$_2$ [52,53] and TiO$_2$ [54,55]. This is usually manifested by simultaneous increase of sensor response, S, and reduction of recovery time, t_{rec}. However, results of the present study exhibit substantial discrepancies from the published results, leading us to suggest that the diversity among different nanostructured nanomaterial could result in different combinations of various physiochemical mechanisms and eventually determine their overall gas sensing performance. As such, the impact of UV illumination on the gas sensing properties would vary from one to another.

Let us summarize the related findings first. Figs.10a and b show the sensor response of a Pd/ns-ZnO film measured at 20 ^{o}C and 80 ^{o}C, respectively, with UV illumination applied in each case. The values of S, t_{res} and t_{rec} derived in the two cases are listed in Table 1. At 20 ^{o}C, the use of UV illumination just increased S slightly from 82 to 85, but t_{rec} became much longer to exceed 24 hours. On the other hand, at 80 ^{o}C, the use of UV illumination caused S to decrease significantly from ~3540 to ~580, and t_{rec} only increased slightly from 18 s to 22

s. The following discussion is performed to interpret and seek deeper insights on the observed gas sensing properties of the Pd/ns-ZnO film.

(i) In the dark and at zero H_2 concentration, the oxygen molecules chemisorbed on ZnO surface extract electrons from the conduction band and become O_2^- ions (Eq. (1)) [22]. A built-in electric field pointing from the interior of a nanocluster to its surface is established. A highly resistive electron depletion region is formed on the nanocluster's surface. At this moment, the resistance of the Pd/ns-ZnO film is high.

$$O_{2\,(gas)} + e^- \rightarrow O_{2\,(ad)}^- \tag{1}$$

(ii) After turning on the UV light, photo electron-hole (e^--h^+) pairs are generated (Eq. (2)). Part of them would recombine directly through band-to-band recombination. The remaining e^--h^+ pairs are separated by the built-in electric field, where holes are driven to migrate towards the nanocluster surface [56-58]. Meanwhile, the holes could be captured by the deep or shallow recombination centers to recombine and consume electrons present around the nanocluster surface [58]. Once the holes reach the surface, they will react with the chemisorbed O_2^- and release O_2 gas molecules (Eq. (3)). Electrons are released to the nanoclusters and contribute to the electrical conduction process. The film resistance drops as a consequence [56-58].

$$hv \rightarrow e^- + h^+ \tag{2}$$

$$h^+ + O_{2\,(ad)}^- \rightarrow O_{2\,(gas)} \tag{3}$$

Concurrently, O_2 molecules in the surrounding would continuously be adsorbed on the ZnO oxide surface and capture free electrons. It is generally believed that $O_{2\,(hv)}^-$ ions are created (Eq. 4)) [50,51]. The UV photons could further dissociate O_2^- ions to produce more reactive O^- ions (Eq. (5)), [54]. These ions are referred to as photo-induced oxygen ions in literatures.

$$O_2 \text{ (gas)} + e^- \rightarrow O_2^-{}_{(hv)} \tag{4}$$

$$O_2^- + e^- \rightarrow 2O^-{}_{(hv)} \tag{5}$$

In addition, some e^- are trapped in shallow states near the bottom of the conduction band. The trap states form an electron storehouse for capturing and releasing free e^- throughout the sensing process (Eq. 6). The trapped electrons can be re-excited to the conduction band via thermal activation process [58], such that the recovery time at low temperature is very long.

$$e^- + \text{shallow } e^- \text{ trap} \leftrightarrow e^-{}_{\text{trap}} + \text{heat} \tag{6}$$
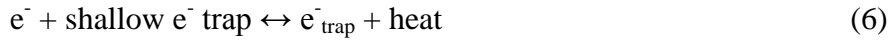
(iii) With the presence of H_2 gas, the catalytic Pd dissociates the molecules into H atoms (Eq. 7) [19], which diffuse onto the ZnO surface and react with chemisorbed oxygen ions (Eqs. 8-9). When they react with the adsorbed oxygen ions, electrons are released to the nanoclusters to result in an increase in conduction electron concentration and reduction of the thickness of the depletion layer on the nanocluster surfaces. The film resistance would drop as a consequence.

$$H_2 \text{ (ad)} \rightarrow 2H_{\text{atom (ad)}} \tag{7}$$

$$4H_{\text{atom (ad)}} + O_2^-{}_{(\text{ad or } hv)} \rightarrow 2H_2O_{\text{ (gas)}} + e^- \tag{8}$$

$$2H_{\text{atom (ad)}} + O^-{}_{(hv)} \rightarrow H_2O_{\text{ (gas)}} + e^- \tag{9}$$
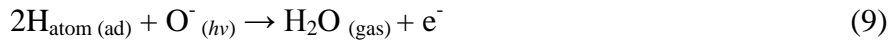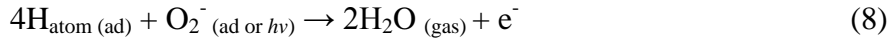
The values of R_{air} and R_{H_2}, and hence the sensor response defined as the ratio of $S \equiv R_{\text{air}}/R_{H_2}$ are jointly determined by some combinations of the above processes. In particular, the value of R_{air} is dominated by reactions (1-6) at the steady state. It generally drops when UV illumination is turned on, because reactions (2-3) prevail. This can be referred to as a mechanism of photo-induced net increase of electron concentration. On the other hand, R_{H_2} is affected by all the reactions (2-9) at the steady state. It also drops when UV illumination is turned on (at any temperature), because the photo-induced oxygen ions ($O_2^-{}_{(hv)}$ and $O^-{}_{(hv)}$) generated by UV photons are more reactive than the chemisorbed oxygen ion ($O_2^-{}_{(\text{ad})}$) which

are the only reactive species existing in the dark environment. This can be referred to as a mechanism of UV enhanced reactivity of chemisorbed oxygen ions. These two mechanisms compete with other to determine the values of R_{air} and R_{H_2}, and finally the value of S.

Consider the case at 20 ^{o}C. When UV light is turned on, R_{air} only reduced to 1/4.4 of the value in dark, but R_{H_2} is reduced by a factor of 1/4.6. This means that the mechanism of UV enhanced reactivity of photo-induced oxygen ions prevails at 20 ^{o}C [49,53,54], and the S would be increased as a consequence.

Next, consider the case at 80 ^{o}C. When UV light is turned on, R_{H_2} reduced significantly to 1/14 of the value in dark, but R_{H_2} only decreased slightly by a factor of 1/2.3. As such, the value of S decreased prominently from ~3540 to ~580. The abrupt decease of R_{air} caused by UV illumination may be due to the effective release of electrons from the shallow trap states and results in a substantial increase in conduction electron concentration. This conjecture is further supported by the shorter t_{rec} observed at 80 ^{o}C, both with and without UV irradiation.

Noticing that t_{rec} detected at 20 ^{o}C and 80 ^{o}C are minute-long, we believe that reaction (6) is always taking place. After turning off the UV light, the trapped electrons require to go through a thermal activation process for the residual photocurrent to extinct. This takes a longer time at a low temperature environment, explaining why the decaying rate is so slow at 20 ^{o}C.

Even though the S and t_{rec} achieved under UV illumination seem to be inferior to those achieved in dark, UV irradiation improves the stability of Pd/ns-ZnO film sensor. Figs. 11a-b show typical results of two stability tests performed on the same sample without and with UV illumination, respective. Without UV assist, the R_{air} value of the Pd/ns-ZnO film drifts progressively to exhibit some increase in the course of measurement, whereas the value of R_{H_2} remains unchanged. To explain this phenomenon, we consider that the Pd/ns-ZnO film is

14

a bilayer structure where the oxide layer has a very high resistance in air. Hence the overall film resistance is greatly affected by the presence of the Pd capping layer. Since Pd is brittle and could be cracked to some extent when repeatedly exposed to high concentration H_2 [59,60], the drift of R_{air} could therefore be attributed to the fragmentation of the Pd layer. The use of UV assist seems to alleviate this drawback. As shown in Fig. 11b, the R_{air} value measured under the UV light is overwhelmed by the photocurrent, which is clamped at a constant level ~2 GΩ. The sensor response of the Pd/ns-ZnO film sensor appears to be highly repeatable. An additional advantage of applying UV assist is to ease the measurement of a low R_{air} without requiring the use of an expensive high-input-impedance electrometer.

4. Conclusion

A nanosponge-like ZnO film with an overall porosity of 73 % composed of loosely connected 13-nm nanoclusters was produced by supersonic cluster beam deposition (SCBD) method and subsequent post-annealing. Attributed to the highly porous structure, the Pd/ns-ZnO film exhibited a short response time ≈1 s for the detection of 2 % H_2 in air at 20

o

 C. The sensor performance was further improved substantially by slightly heating the film sensor to 80 °C. Its sensing performance acquired at 80 °C is better than those of many other nano-MO_x based H_2 sensors operating at temperatures > 200 °C. UV irradiation showed negative effect on S and t_{rec} while t_{res} was effectively unaffected. The decrease of S is mainly due to the decrease of R_{air} under UV light. The retardation of the unloading process, namely long recovery time, can be attributed to the prolonged thermal release of electrons captured by shallow e⁻ traps. Furthermore, UV irradiation clamps the value of R_{air} at ~2 GΩ, which helps to improve the sensor stability by covering up the drift of R_{air} associatewith the

fragmentation of the Pd capping layer, and to ease the measurement of resistive sensing signal without requiring the use of an expensive high-input-impedance electrometer.

Acknowledgements

References

[1] J. Tollefson, Fuel of the Future?, Nature 464 (2010) 1262-1264.

[2] K. Mazloomi, C. Gomes, Hydrogen as an energy carrier: Prospects and challenges, Renew. Sust. Energ. Rev. 16 (2012) 3024-3033.

[3] L. Boon-Brett, J. Bousek, G. Black, P. Moretto, P. Castello, T. Hubert, U. Banach, Identifying performance gaps in hydrogen safety sensor technology for automotive and stationary applications, Int. J. Hydrogen Energ. 35 (2010) 373-384.

[4] F. Yang, D.K. Taggart, R.M. Penner, Joule heating a palladium nanowire sensor for accelerated response and recovery to hydrogen gas, Small 6 (2010) 1422-1429.

[5] T. Hubert, L. Boon-Brett, G. Black, U. Banach, Hydrogen sensors - A review, Sens. Actuators B 157 (2011) 329-352.

[6] W.J. Buttner, M.B. Post, R. Burgess, C. Rivkin, An overview of hydrogen safety sensors and requirements, Int. J. Hydrogen Energ. 36 (2011) 2462-2470.

[7] A. Somov, A. Baranov, A. Savkin, D. Spirjakin, A. Spirjakin, R. Passerone, Development of wireless sensor network for combustible gas monitoring, Sens. Actuators A 171 (2011) 398-405.

[8] G. Korotcenkov, B.K. Cho, Instability of metal oxide-based conductometric gas sensors and approaches to stability improvement, Sens. Actuators B 156 (2011) 527-538.

[9] T. Hyodo, T. Yamashita, Y. Shimizu, Effects of surface modification of noble-metal sensing electrodes with Au on the hydrogen-sensing properties of diode-type gas sensors employing an anodized titania film, Sens. Actuators B 207 (2015) 105-116.

[10] A. Sanger, A. Kumar, A. Kumar, R. Chandra, Highly sensitive and selective hydrogen gas sensor using sputtered grown Pd decorated MnO_2 nanowalls, Sens. Actuators B 234 (2016) 8-14.

[11] X.H. Xia, W.X. Wu, Z. Wang, Y.W. Bao, Z.B. Huang, Y. Gao, A hydrogen sensor based on orientation aligned TiO_2 thin films with low concentration detecting limit and short response time, Sens. Actuators B 234 (2016) 192-200.

[12] J. Moon, H.P. Hedman, M. Kemell, A. Tuominen, R. Punkkinen, Hydrogen sensor of Pd-decorated tubular TiO_2 layer prepared by anodization with patterned electrodes on SiO_2/Si substrate, Sens. Actuators B 222 (2016) 190-197.

[13] M. Zhao, J.X. Huang, C.W. Ong, Feasibility of H_2 sensors composed of tungsten oxide nanocluster films, Int. J. Hydrogen Energ. 38 (2013) 15559-15566.

[14] M. Zhao, M.H. Wong, J.X. Huang, C.W. Ong, Ultrathin percolated WO_3 cluster film and its resistive response to H_2, J. Alloy. Compd. 612 (2014) 163-169.

[15] J.J. Wu, D.W. Zeng, S.Q. Tian, K. Xu, D.G. Li, C.S. Xie, Competitive influence of surface area and mesopore size on gas-sensing properties of SnO_2 hollow fibers, J. Mater. Sci. 50 (2015) 7725-7734.

[16] Y. Shimizu, Y. Nakamura, M. Egashira, Effects of diffusivity of hydrogen and oxygen through pores of thick-film SnO_2-based sensors on their sensing properties, Sens. Actuators B 13 (1993) 128-131.

[17] Y. Shimizu, T. Maekawa, Y. Nakamura, M. Egashira, Effects of gas diffusivity and reactivity on sensing properties of thick film SnO_2-based sensors, Sens. Actuators B 46 (1998) 163-168.

[18] N. Matsunaga, G. Sakai, K. Shimanoe, N. Yamazoe, Formulation of gas diffusion dynamics for thin film semiconductor gas sensor based on simple reaction-diffusion equation, Sens. Actuators B 96 (2003) 226-233.

[19] M. Zhao, J.X. Huang, C.W. Ong, Diffusion-controlled H_2 sensors composed of Pd-coated highly porous WO_3 nanocluster films, Sens. Actuators B 191 (2014) 711-718.

[20] M.E. Franke, T.J. Koplin, U. Simon, Metal and metal oxide nanoparticles in chemiresistors: Does the nanoscale matter?, Small 2 (2006) 36-50.

[21] N. Yamazoe, New approaches for improving semiconductor gas sensors, Sens. Actuators B 5 (1991) 7-19.

[22] N. Barsan, D. Koziej, U. Weimar, Metal oxide-based gas sensor research: How to?, Sens. Actuators B 121 (2007) 18-35.

[23] G. Korotcenkov, Metal oxides for solid-state gas sensors: What determines our choice?, Mat. Sci. Eng. B 139 (2007) 1-23.

[24] M. Zhao, J.X. Huang, C.W. Ong, Preparation and structure dependence of H_2 sensing properties of palladium-coated tungsten oxide films, Sens. Actuators B 177 (2013) 1062-1070.

[25] S. Shukla, S. Seal, L. Ludwig, C. Parish, Nanocrystalline indium oxide-doped tin oxide thin film as low temperature hydrogen sensor, Sens. Actuators B 97 (2004) 256-265.

[26] S. Fardindoost, A.I. Zad, F. Rahimi, R. Ghasempour, Pd doped WO_3 films prepared by sol-gel process for hydrogen sensing, Int. J. Hydrogen Energ. 35 (2010) 854-860.

[27] O. Lupan, L. Chow, T. Pauporté, L.K. Ono, B. Roldan Cuenya, G. Chai, Highly sensitive and selective hydrogen single-nanowire nanosensor, Sens. Actuators B 173 (2012) 772-780.

[28] L.L. Fields, J.P. Zheng, Y. Cheng, P. Xiong, Room-temperature low-power hydrogen sensor based on a single tin dioxide nanobelt, Appl. Phys. Lett. 88 (2006) 263102.

[29] O. Lupan, V.V. Ursaki, G. Chai, L. Chow, G.A. Emelchenko, I.M. Tiginyanu, A.N. Gruzintsev, A.N. Redkin, Selective hydrogen gas nanosensor using individual ZnO nanowire with fast response at room temperature, Sens. Actuators B 144 (2010) 56-66.

[30] K. Wegner, P. Piseri, H.V. Tafreshi, P. Milani, Cluster beam deposition: a tool for nanoscale science and technology, J. Phys. D Appl. Phys. 39 (2006) R439-R459.

[31] M. Zhao, J.X. Huang, M.H. Wong, Y.M. Tang, C.W. Ong, Versatile computer-controlled system for characterization of gas sensing materials, Rev. Sci. Instrum. 82 (2011) 105001.

[32] Z. Wang, Y.M. Hu, W. Wang, X. Zhang, B.X. Wang, H.Y. Tian, Y. Wang, J.G. Guan, H.S. Gu, Fast and highly-sensitive hydrogen sensing of Nb_2O_5 nanowires at room temperature, Int. J. Hydrogen Energ. 37 (2012) 4526-4532.

[33] J.J. Hassan, M.A. Mahdi, C.W. Chin, H. Abu-Hassan, Z. Hassan, Room temperature hydrogen gas sensor based on ZnO nanorod arrays grown on a SiO_2/Si substrate via a microwave-assisted chemical solution method, J. Alloy. Compd. 546 (2013) 107-111.

[34] J.J. Hassan, M.A. Mahdi, C.W. Chin, H. Abu-Hassan, Z. Hassan, A high-sensitivity room-temperature hydrogen gas sensor based on oblique and vertical ZnO nanorod arrays, Sens. Actuators B 176 (2013) 360-367.

[35] Y. Wang, B. Liu, D. Cai, H. Li, Y. Liu, D. Wang, L. Wang, Q. Li, T. Wang, Room-temperature hydrogen sensor based on grain-boundary controlled Pt decorated In_2O_3 nanocubes, Sens. Actuators B 201 (2014) 351-359.

[36] C. Xiang, Z. She, Y. Zou, J. Cheng, H. Chu, S. Qiu, H. Zhang, L. Sun, F. Xu, A room-temperature hydrogen sensor based on Pd nanoparticles doped TiO_2 nanotubes, Ceram. Int. 40 (2014) 16343-16348.

[37] M. Zhao, C.W. Ong, Improved H_2-sensing performance of nanocluster-based highly porous tungsten oxide films operating at moderate temperature, Sens. Actuators B 174 (2012) 65-73.

[38] S.P. Zhang, T. Lei, D. Li, G.Z. Zhang, C.S. Xie, UV light activation of TiO_2 for sensing formaldehyde: How to be sensitive, recovering fast, and humidity less sensitive, Sens. Actuators B 202 (2014) 964-970.

[39] N. Barsan, U. Weimar, Conduction model of metal oxide gas sensors, J. Electroceram. 7 (2001) 143-167.

[40] G.N. Chaudhari, A.M. Bende, A.B. Bodade, S.S. Patil, V.S. Sapkal, Structural and gas sensing properties of nanocrystalline TiO_2:WO_3-based hydrogen sensors, Sens. Actuators B 115 (2006) 297-302.

[41] E. Ghadiri, A. Iraji zad, F. Razi, Hydrogen sensing properties of pure and Pd activated WO_3 nanostructured films, Synth. React. Inorg. Me. 37 (2007) 453-456.

[42] J.W. Gong, J.R. Sun, Q.F. Chen, Micromachined sol-gel carbon nanotube/SnO_2 nanocomposite hydrogen sensor, Sens. Actuators B 130 (2008) 829-835.

[43] S.J. Ippolito, S. Kandasamy, K. Kalantar-zadeh, W. Wlodarski, Hydrogen sensing characteristics of WO_3 thin film conductometric sensors activated by Pt and Au catalysts, Sens. Actuators B 108 (2005) 154-158.

[44] R. Ghasempour, A. Iraji zad, Hybrid multiwalled carbon nanotubes and trioxide tungsten nanoparticles for hydrogen gas sensing, J. Phys. D Appl. Phys. 42 (2009) 165105.

[45] K. Mukherjee, S.B. Majumder, Hydrogen sensing characteristics of wet chemical synthesized tailored $Mg_{0.5}Zn_{0.5}Fe_2O_4$ nanostructures, Nanotechnology, 21 (2010) 255504.

[46]Z. Wang, Z. Li, T. Jiang, X. Xu, C. Wang, Ultrasensitive hydrogen sensor based on

Pd^0-loaded SnO_2 electrospun nanofibers at room temperature, ACS Appl. Mater. Inter. 5

(2013) 2013-2021.

[47]B. Wang, L.F. Zhu, Y.H. Yang, N.S. Xu, G.W. Yang, Fabrication of a SnO_2 nanowire

gas sensor and sensor performance for hydrogen, J. Phys. Chem. C 112 (2008)

6643-6647.

[48]S. Park, T. Hong, J. Jung, C. Lee, Room temperature hydrogen sensing of multiple

networked ZnO/WO_3 core–shell nanowire sensors under UV illumination, Curr. Appl.

Phys. 14 (2014) 1171-1175.

[49]N.M. Kiasari, S. Soltanian, B. Gholamkhass, P. Servati, Environmental gas and light

sensing using ZnO nanowires, IEEE T. Nanotechnol. 13 (2014) 368-374.

[50]S.W. Fan, A.K. Srivastava, V.P. Dravid, UV-activated room-temperature gas sensing

mechanism of polycrystalline ZnO, Appl. Phys. Lett. 95 (2009) 142106.

[51]H. Ahn, Y.Q. Wang, S.H. Jee, M. Park, Y.S. Yoon, D.J. Kim, Enhanced UV activation of

electrochemically doped Ni in ZnO nanorods for room temperature acetone sensing,

Chem. Phys. Lett. 511 (2011) 331-335.

[52]D. Ao, M. Ichimura, UV irradiation effects on hydrogen sensors based on SnO_2 thin

films fabricated by the photochemical deposition, Solid State Electron. 69 (2012) 1-3.

[53]T. Li, W. Zeng, D. Shi, S. Hussain, UV-enhanced hydrogen sensor based on

nanocone-assembled 3D SnO_2 at low temperature, Mater. Lett. 161 (2015) 648-651.

[54]T.Y. Yang, H.M. Lin, B.Y. Wei, C.Y. Wu, C.K. Lin, UV enhancement of the gas sensing

properties of nano-TiO_2, Rev. Adv. Mater. Sci 4 (2003) 48-54.

[55]C.H. Han, D.W. Hong, S.D. Han, J. Gwak, K.C. Singh, Catalytic combustion type

hydrogen gas sensor using TiO_2 and UV-LED, Sens. Actuators B 125 (2007) 224-228.

[56]O. Lupan, L. Chow, G.Y. Chai, A single ZnO tetrapod-based sensor, Sens. Actuators B

141 (2009) 511-517.

[57]J. Cui, D. Wang, T. Xie, Y. Lin, Study on photoelectric gas-sensing property and

photogenerated carrier behavior of Ag–ZnO at the room temperature, Sens. Actuators B

186 (2013) 165-171.

[58]S.S. Zhang, C.S. Xie, Z.J. Zou, L. Yang, H.Y. Li, S.P. Zhang, High photoconductive

response of gas-sensitized porous nanocrystalline TiO_2 film in formaldehyde ambience

and carrier transport kinetics, J. Phys. Chem. C 116 (2012) 19673-19681.

[59]F. Favier, E.C. Walter, M.P. Zach, T. Benter, R.M. Penner, Hydrogen sensors and

switches from electrodeposited palladium mesowire arrays, Science 293 (2001)

2227-2231.

[60]C.W. Ong, Y.M. Tang, Sputtering pressure dependence of hydrogen-sensing effect of

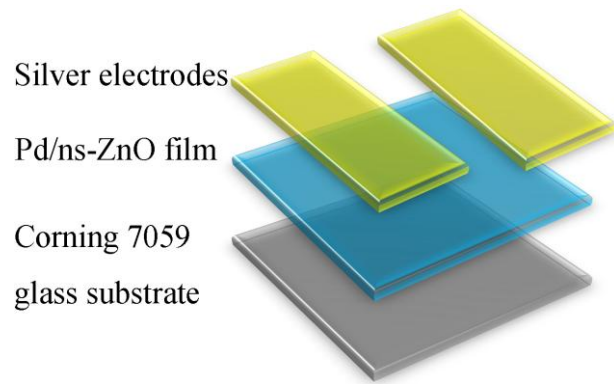palladium films, J. Mater. Res. 24 (2009) 1919-1927.

Figure captions:

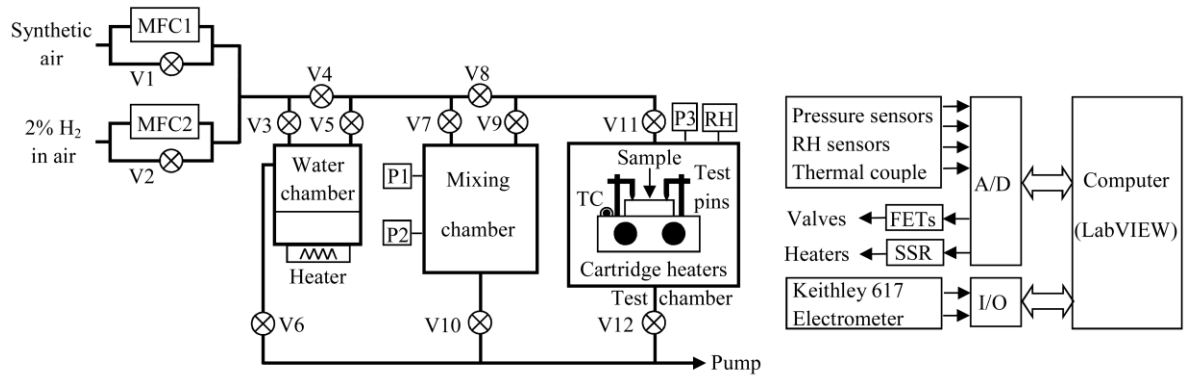**Fig. 1.** Schematic structure of Pd/ns-ZnO film sensor.

Fig. 2. Schematic design of gas sensing measurement system. V: electromagnetic valve; MFC: mass flow controller; P: pressure sensor; RH: relative humidity sensor; TC: thermocouple; A/D: analog digital converter; FET: field effect transistor for valve control; SSR: solid state relay for heater control.
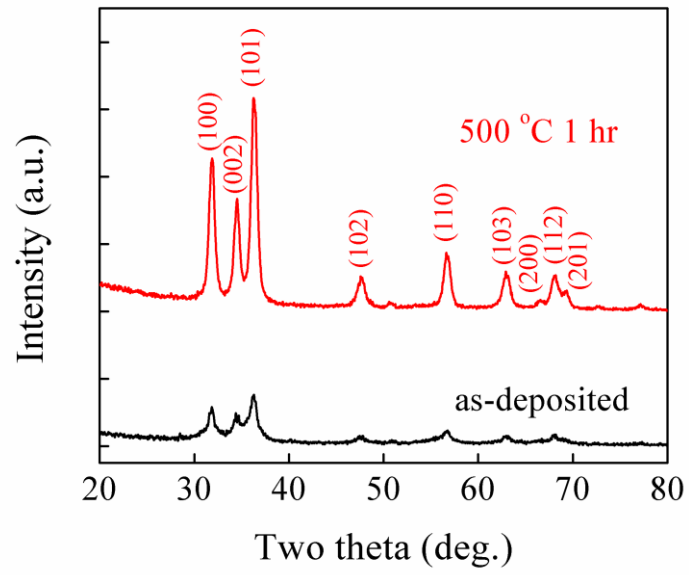
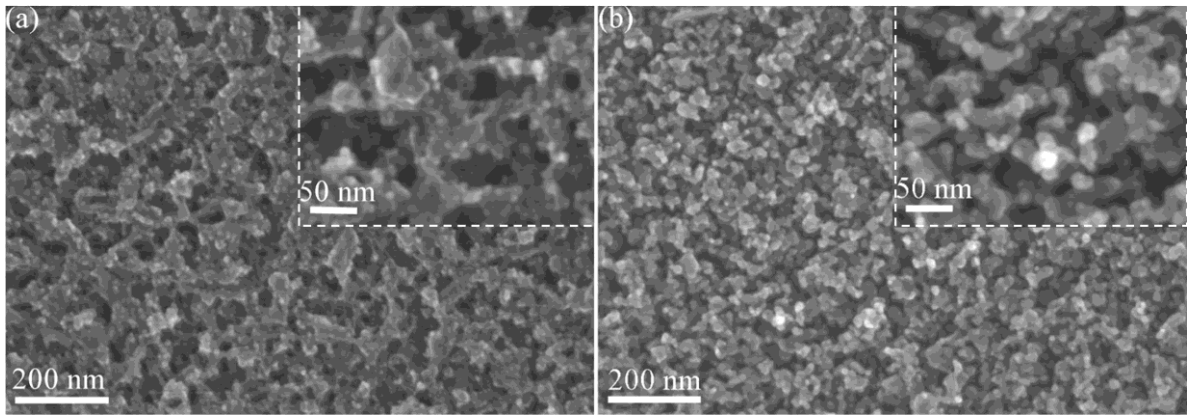**Fig. 3.** XRD spectra of as-deposited and 500 ^{o}C annealed ns-ZnO films.

Fig. 4. SEM images of (a) as-deposited and (b) 500 ^{o}C annealed ns-ZnO films. Insets are images at higher magnification.
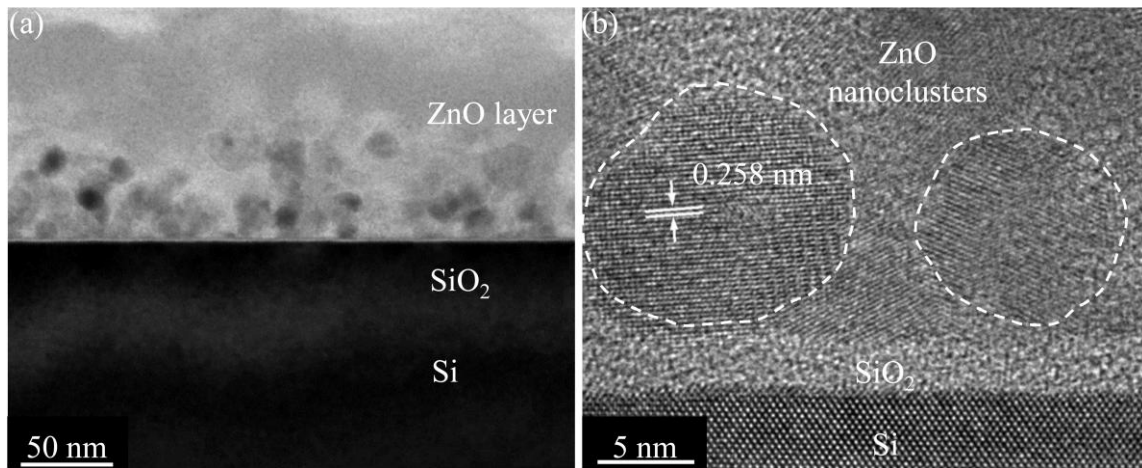
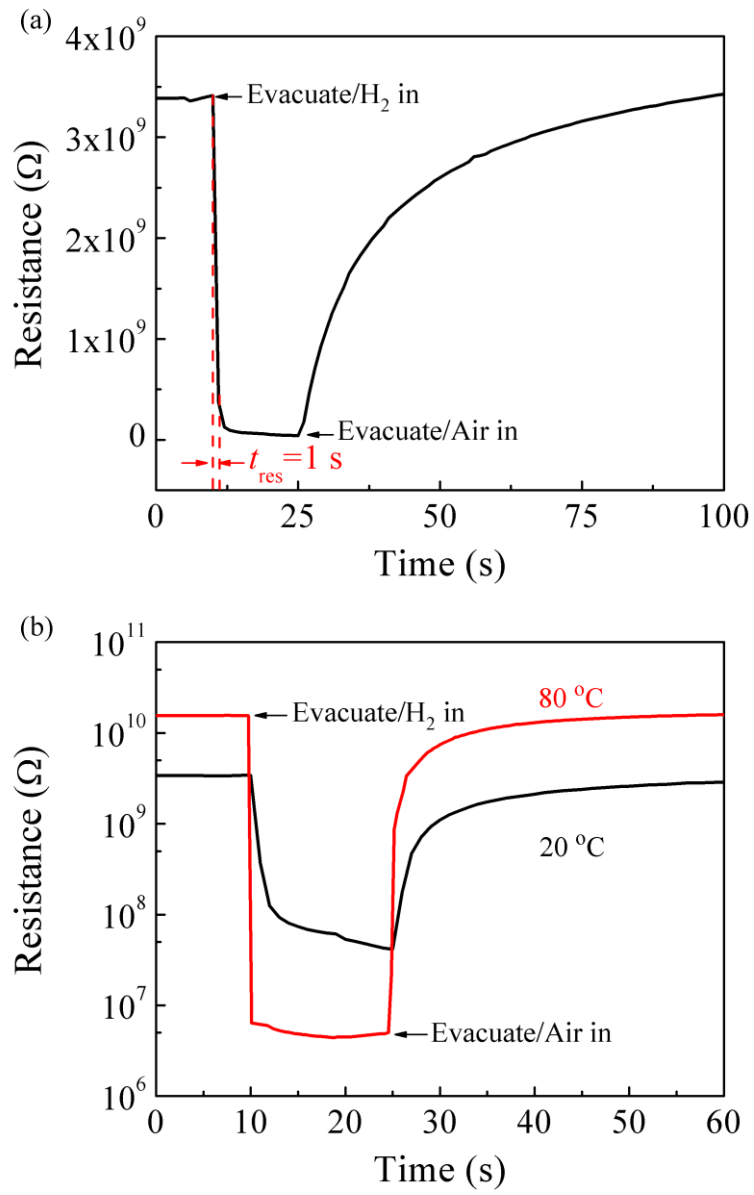**Fig. 5.** Cross-section TEM images of 500 ^{o}C annealed ns-ZnO film.

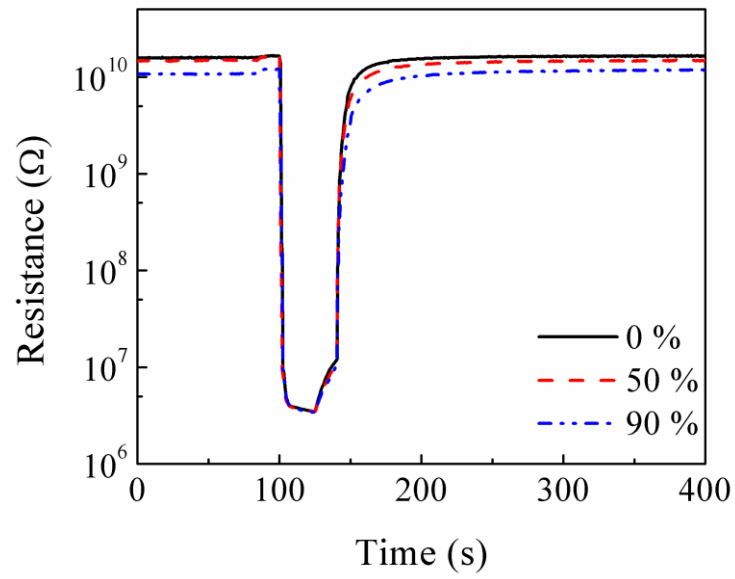**Fig. 6.** Resistive responses of Pd/ns-ZnO film to 2 % H_2 in air at (a) 20 ^{o}C and (b) 80 ^{o}C. **Fig. 7.** Resistive response of Pd/ns-ZnO film to 2 % H_2 in air measured at 0, 50 % and 90 % relative humidity. Data were recorded at 80 ^{o}C.
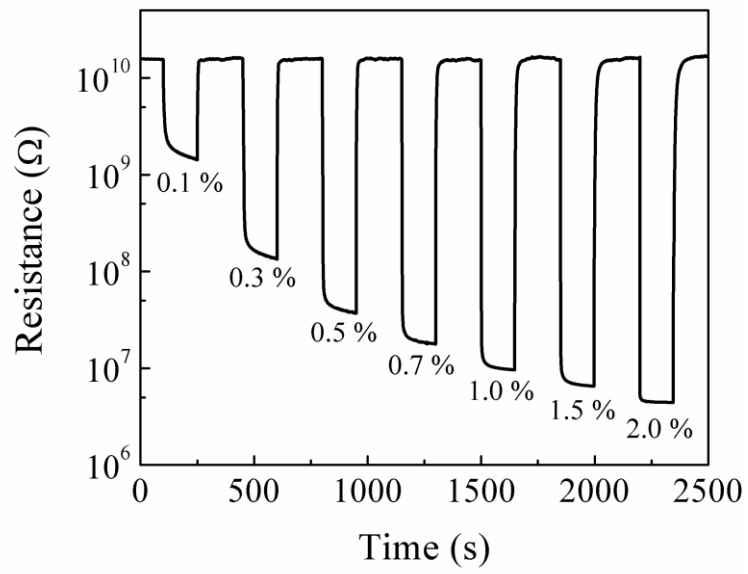
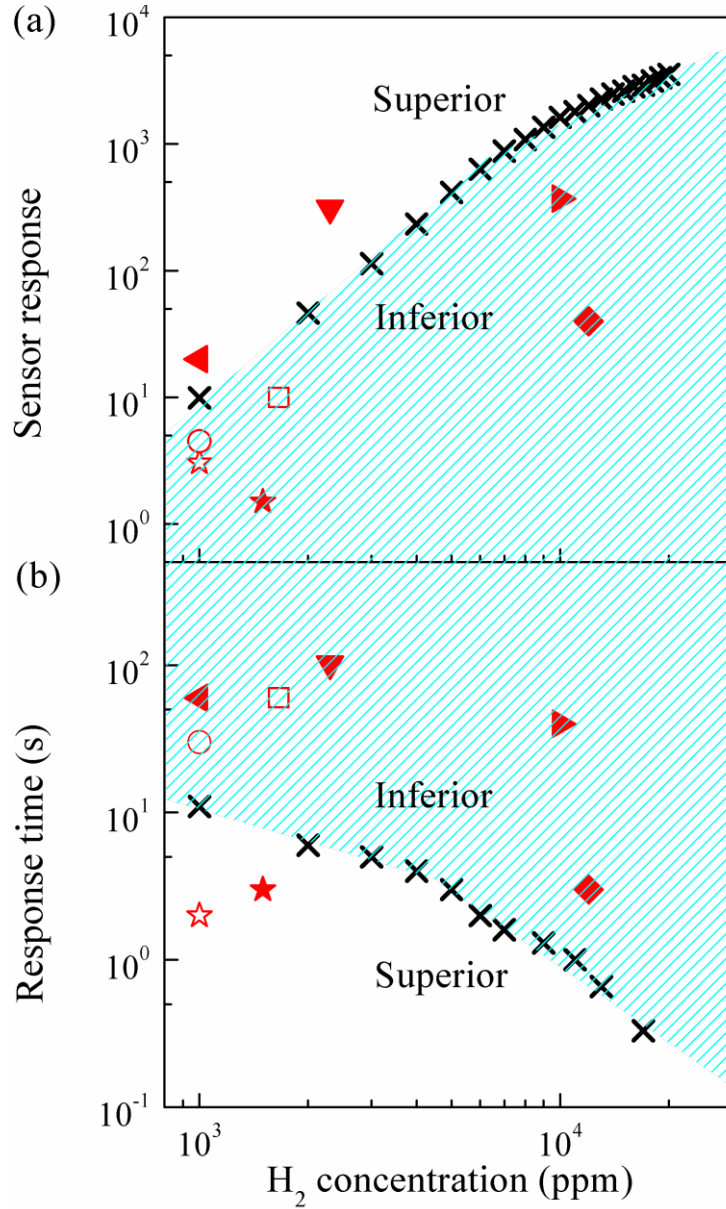**Fig. 8.** Resistive response of Pd/ns-ZnO film to 0.1–2 % H_2 in air measured at 80 ^{o}C.

Fig. 9. Comparison of (a)S and (b)t_{res} of a Pd/SCBD ns-ZnO film measured at 80°C with the published data of various H_2 sensors composed of zero-dimensional (solid symbols) and one-dimensional (hollow symbols) MO_x nanomaterials measured at temperatures > 200 ^{o}C. ×our sample at 80 ^{o}C ◄ Pt-WO$_3$-TiO$_2$ [40] ▼ Pd/WO$_3$ [41] ★ CNT- SnO$_2$ [42] ► Au/WO$_3$ [43] ◆ CNT-WO$_3$ [44] □ MgZnFe$_2$O$_4$ [45] ☆SnO$_2$ [46] ○SnO$_2$ [47]
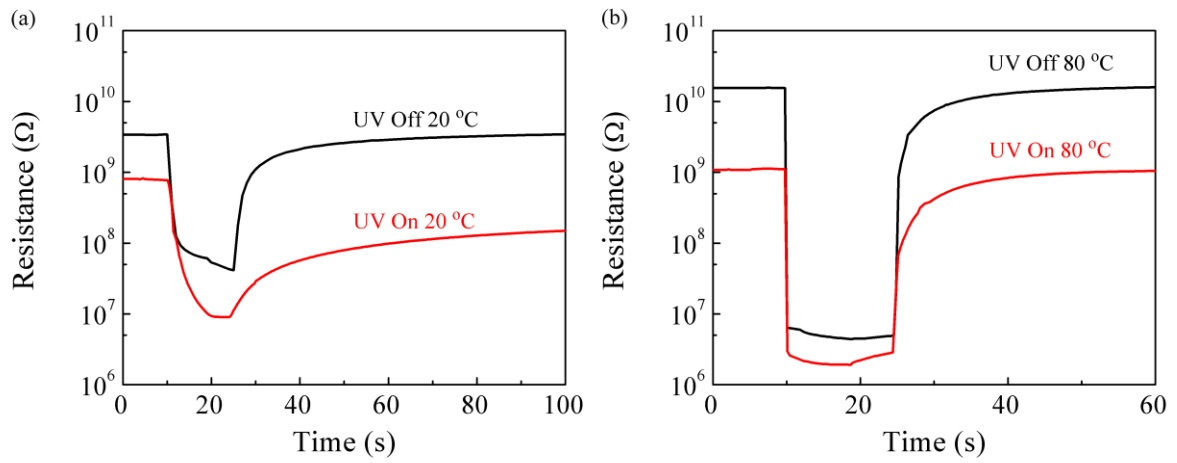
Fig. 10. Comparison of resistive responses of Pd/ns-ZnO film to 2 % H_2 in air with and without UV irradiation measured at (a) 80 $^{\circ}$C and (b) 20 $^{\circ}$C. The power density of UV illumination is 10 mW/cm^2.
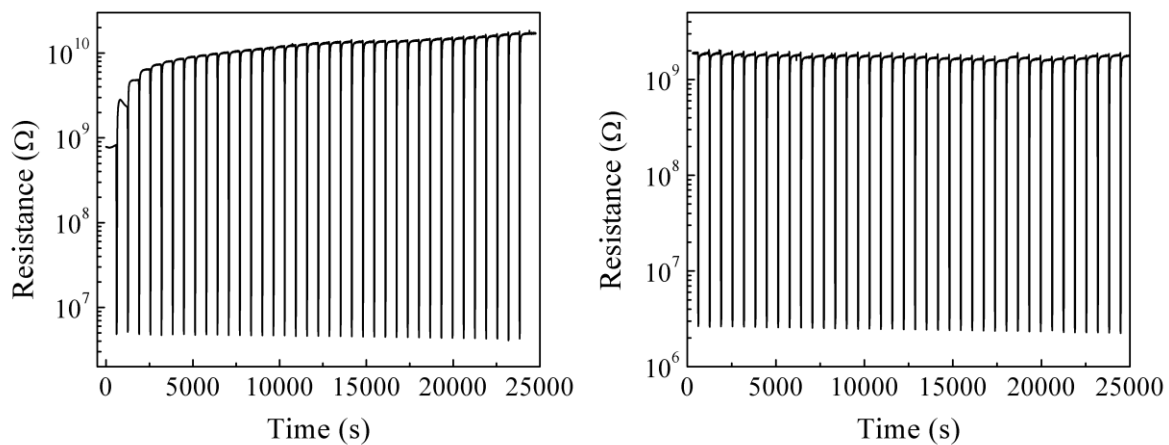
Fig. 11. Accelerated stability test of resistive response of Pd/ns-ZnO film to 2 % H_2 in air performed at 80 $^{\circ}$C (a) without and (b) with UV irradiation. The power density of UV illumination is 10 mW/cm^2.

Table 1 Comparison of sensing parameters to 2 % H_2/air admixture measured at 20 ^{o}C and 80 ^{o}C with and without UV irradiation respectively. The power density of UV illumination is 10 mW/cm^2.

Test condition	R_{air} (GΩ)	R_{H_2} (MΩ)	I_{air} (nA)	I_{H_2} (nA)	S	t_{res} (s)	t_{rec} (s)
UV Off, 80 ^{o}C	15.6	4.41	0.06	227	~3540	0.3	18
UV On, 80 ^{o}C	1.11	1.91	0.90	523	~580	0.3	22
UV Off, 20 ^{o}C	3.41	41.6	0.29	24.0	82	1	52
UV On ,20 ^{o}C	0.77	8.99	1.30	111	85	2	> 24 hrs

Silver electrodes

Pd/ns-ZnO film

Corning 7059
glass substrate

Fig. 1. Schematic structure of Pd/ns-ZnO film sensor.

Fig. 2. Schematic design of gas sensing measurement system. V: electromagnetic valve; MFC: mass flow controller; P: pressure sensor; RH: relative humidity sensor; TC: thermocouple; A/D: analog digital converter; FET: field effect transistor for valve control; SSR: solid state relay for heater control.

Fig. 3. XRD spectra of as-deposited and 500 ^{o}C annealed ns-ZnO films.

Fig. 4. SEM images of (a) as-deposited and (b) 500 ^{o}C annealed ns-ZnO films. Insets are images at higher magnification.

Fig. 5. Cross-section TEM images of 500 $^{\mathrm{o}}$C annealed ns-ZnO film.

Fig. 6. Resistive responses of Pd/ns-ZnO film to 2 % H_2 in air at (a) 20 ^{o}C and (b) 80 ^{o}C.

Fig. 7. Resistive response of Pd/ns-ZnO film to 2 % H_2 in air measured at 0, 50 % and 90 % relative humidity. Data were recorded at 80 ^{o}C.

Fig. 8. Resistive response of Pd/ns-ZnO film to 0.1–2 % H_2 in air measured at 80 ^{o}C.

Fig. 9. Comparison of (a) S and (b) t_{res} of a Pd/SCBD ns-ZnO film measured at 80 °C with the published data of various H_2 sensors composed of zero-dimensional (solid symbols) and one-dimensional (hollow symbols) MO_x nanomaterials measured at temperatures > 200 °C.

×our sample at 80 °C ◄ Pt-WO_3-TiO_2 [40] ▼ Pd/WO_3 [41]　　★ CNT- SnO_2 [42]

► Au/WO_3 [43]　　◆ CNT-WO_3 [44]　□ $MgZnFe_2O_4$ [45]　☆SnO_2 [46] ○SnO_2 [47]

Fig. 10. Comparison of resistive responses of Pd/ns-ZnO film to 2 % H_2 in air with and without UV irradiation measured at (a) 80 ^{o}C and (b) 20 ^{o}C. The power density of UV illumination is 10 mW/cm^2.

Fig. 11. Accelerated stability test of resistive response of Pd/ns-ZnO film to 2 % H_2 in air performed at 80 $^{\circ}$C (a) without and (b) with UV irradiation. The power density of UV illumination is 10 mW/cm^2.

Figure(1)
Click here to download high resolution image

Silver electrodes

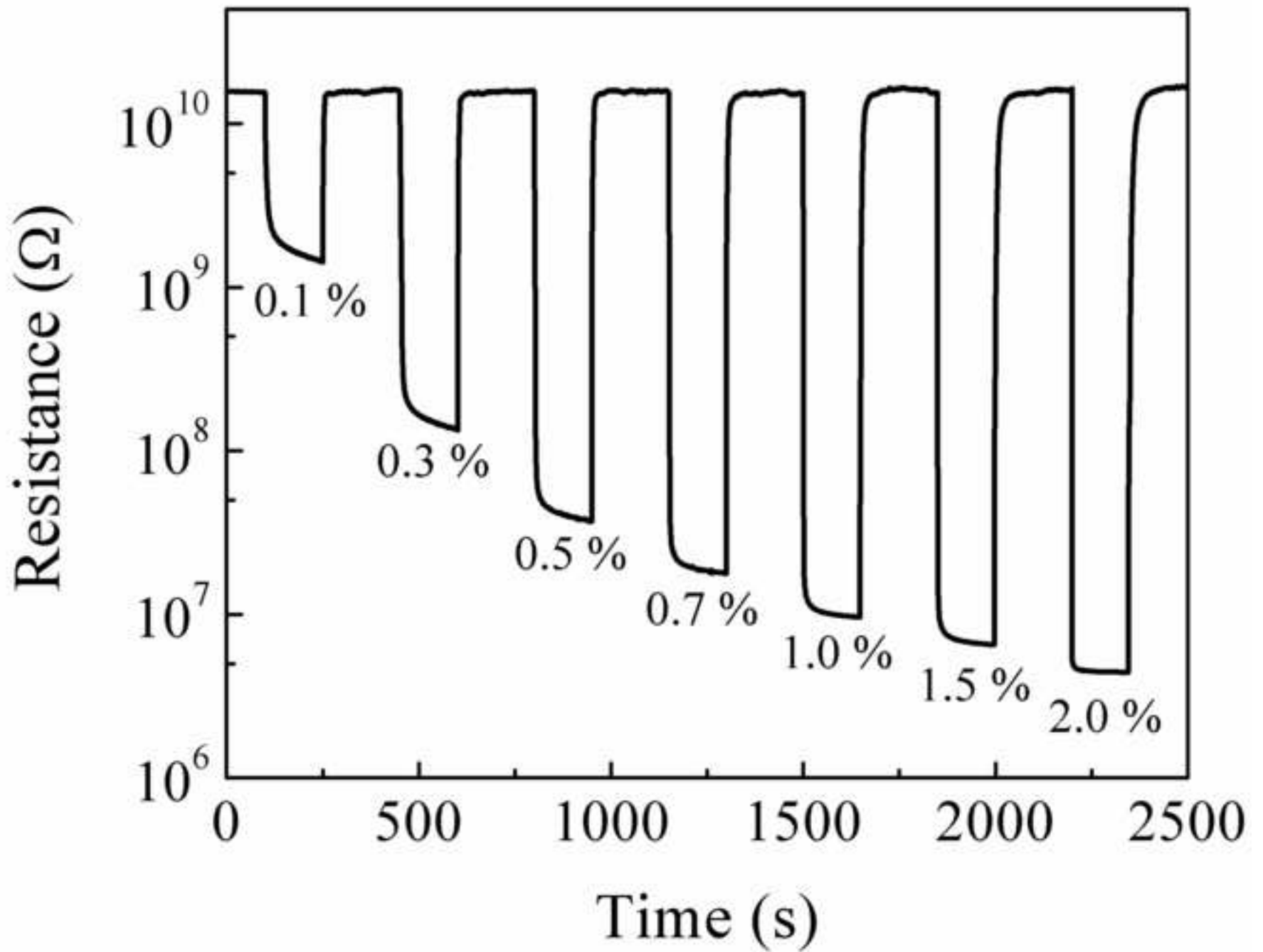Pd/ns-ZnO film

Corning 7059
glass substrate
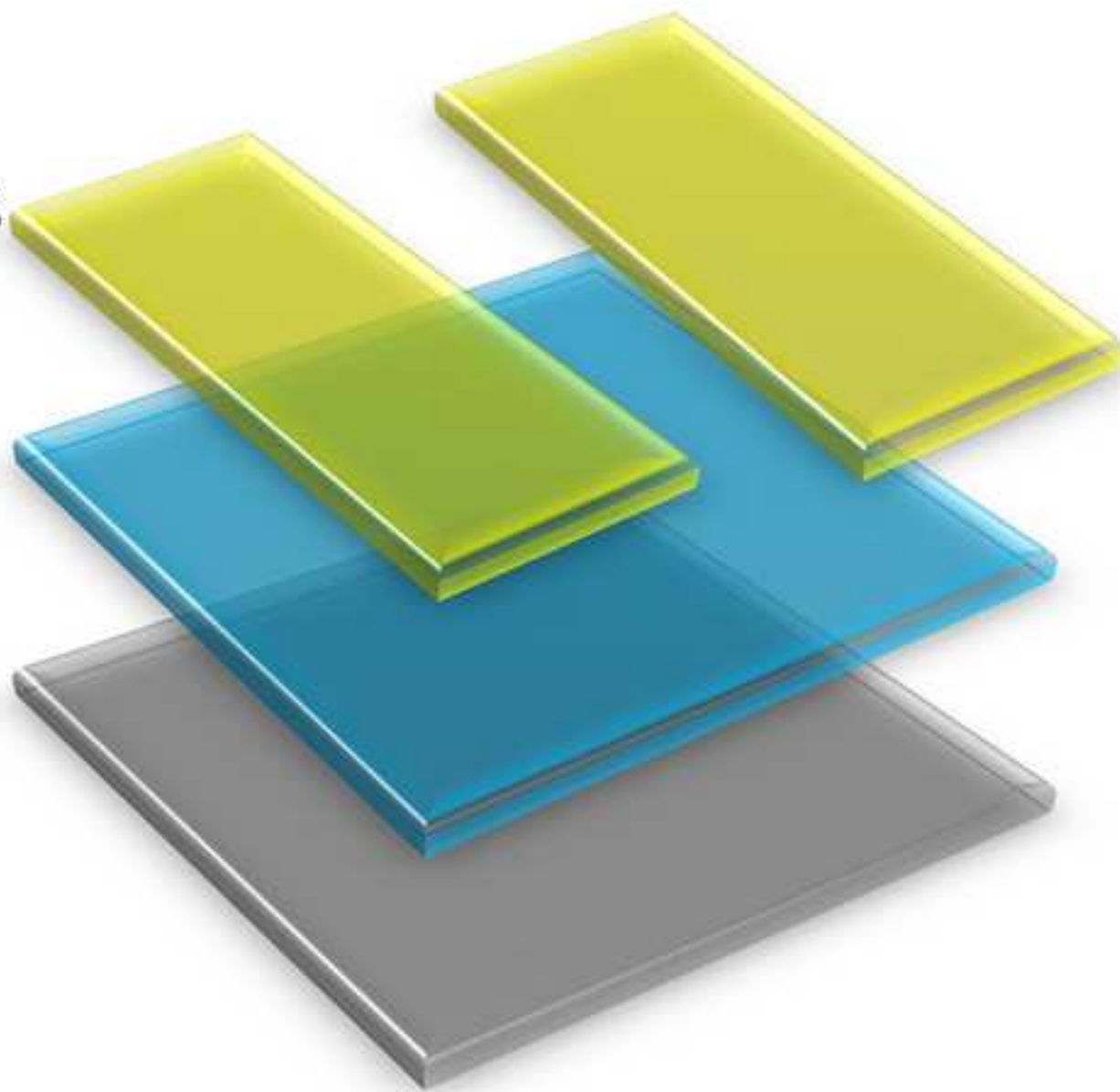
Figure(2)
Click here to download high resolution image
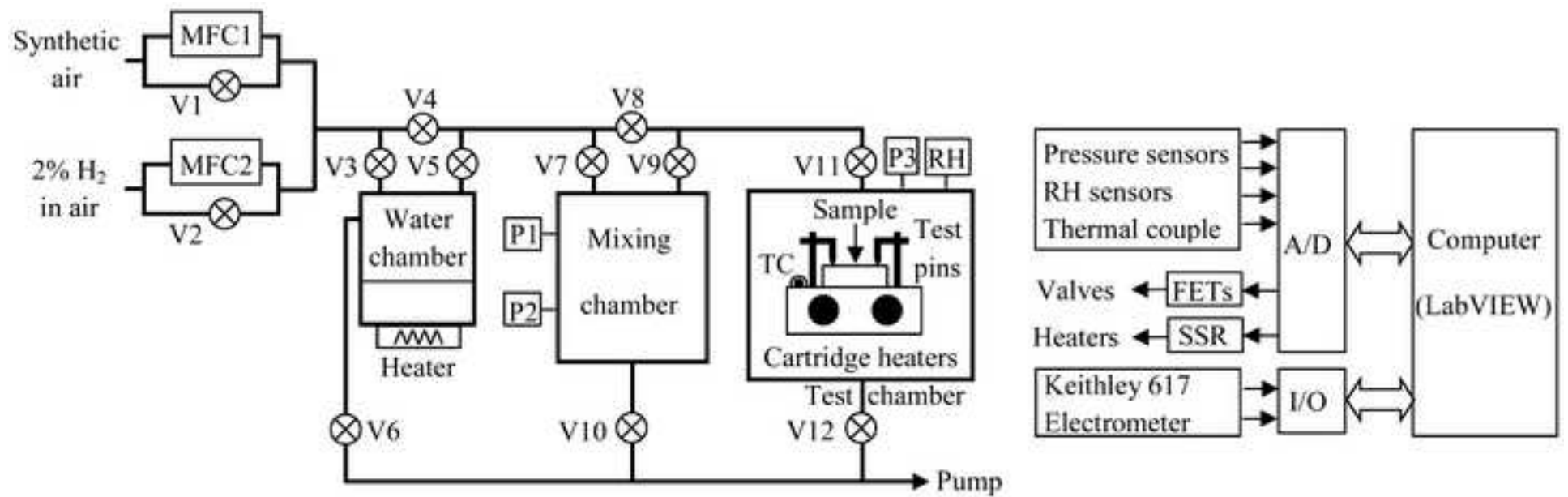
Figure(3)
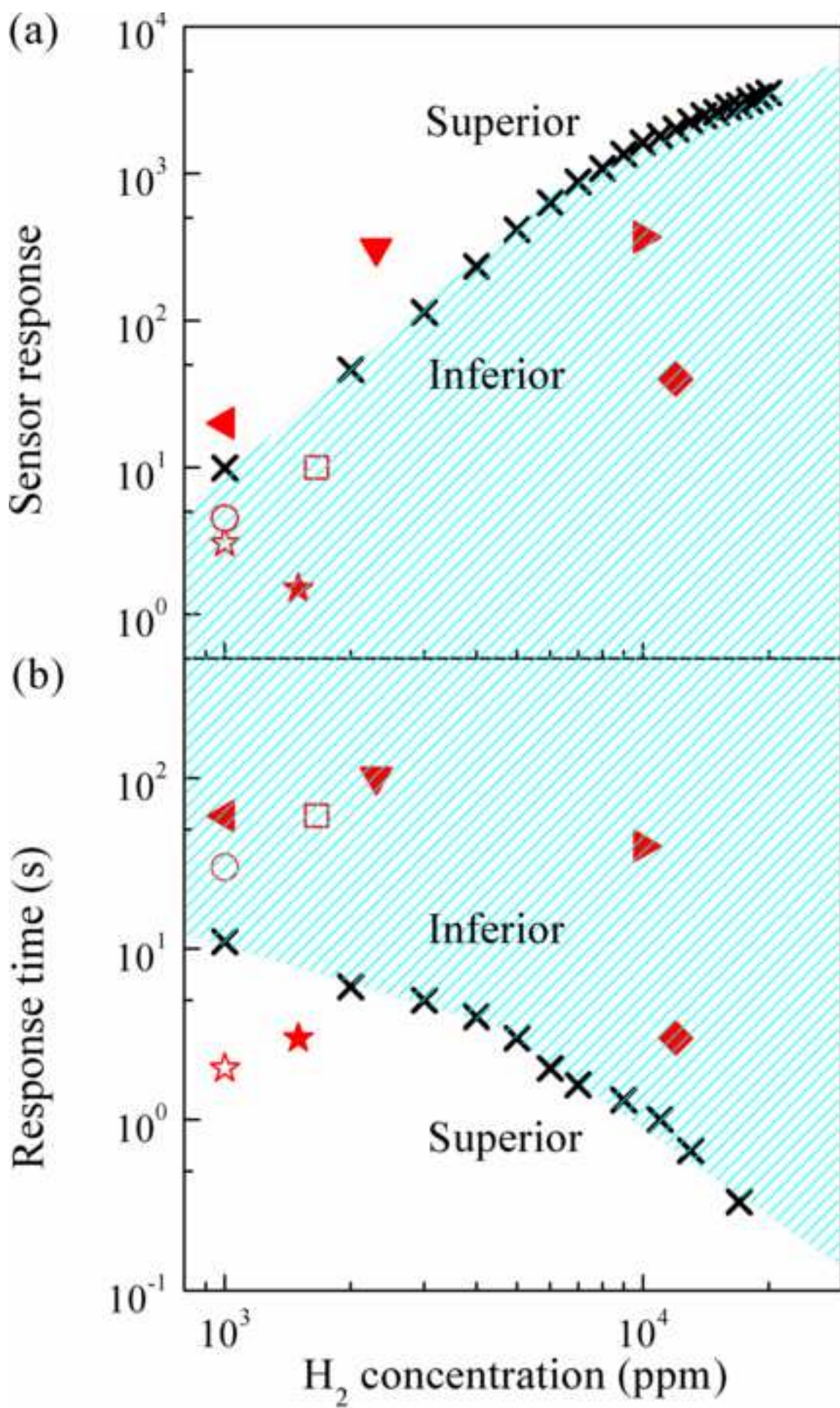**Click here to download high resolution image**
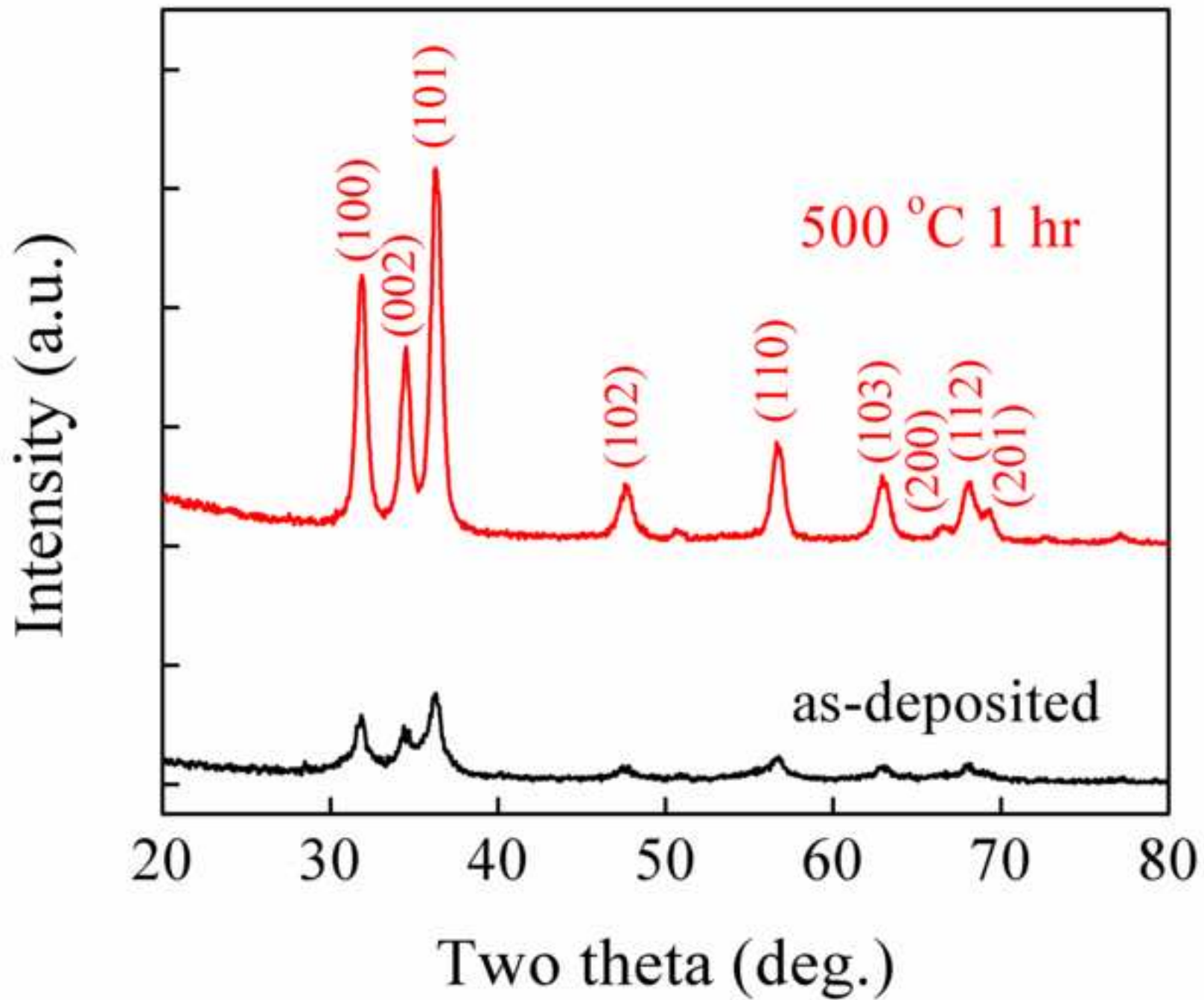
Figure(4)
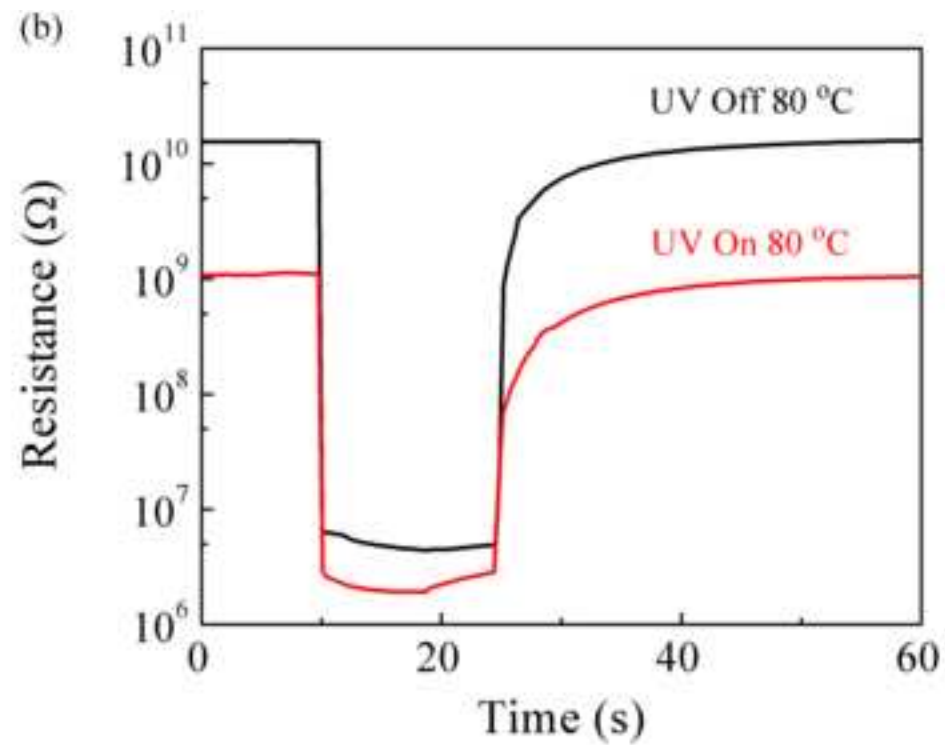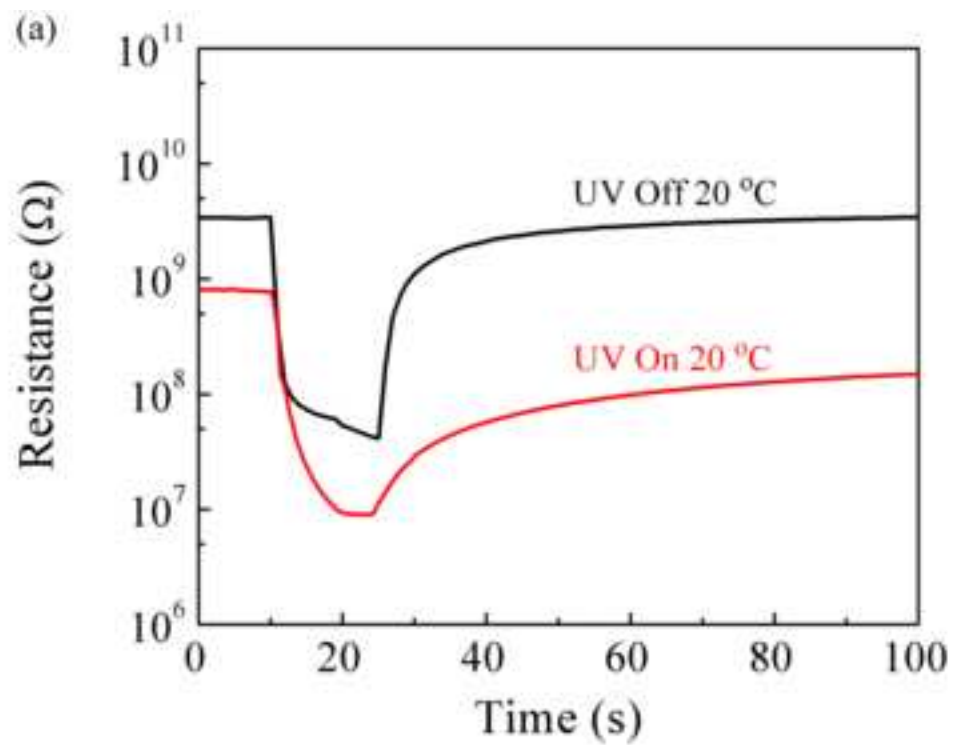**Click here to download high resolution image**
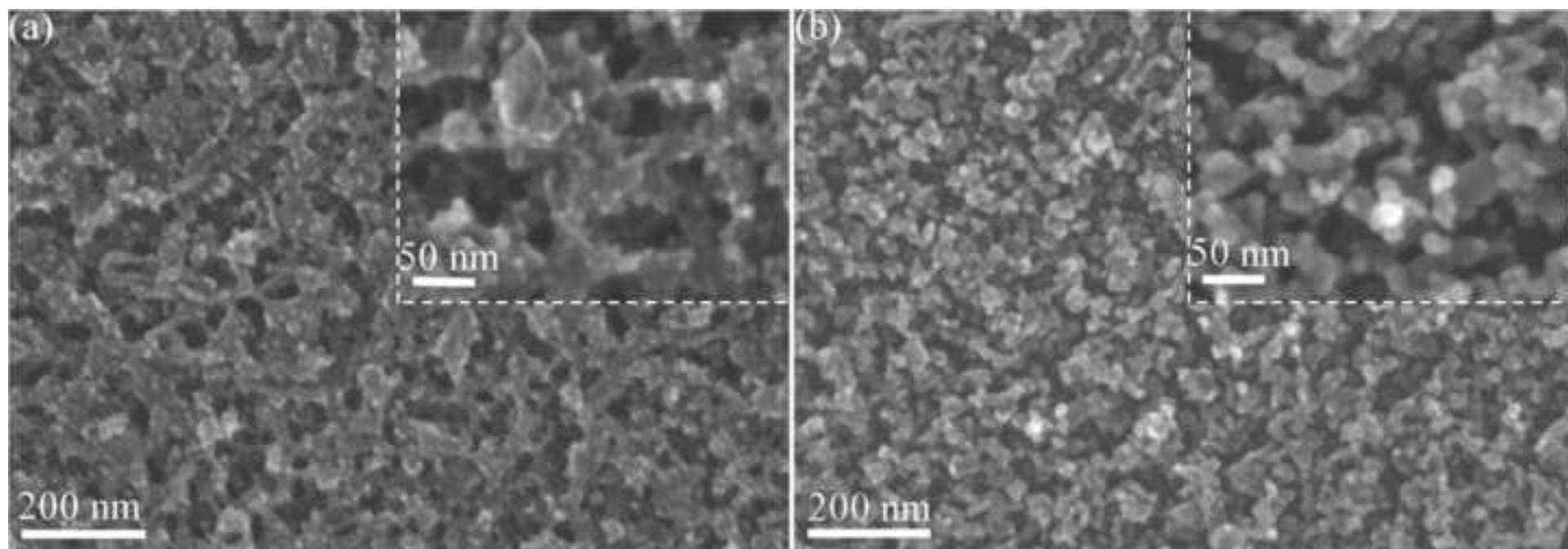
Figure(5)
Click here to download high resolution image
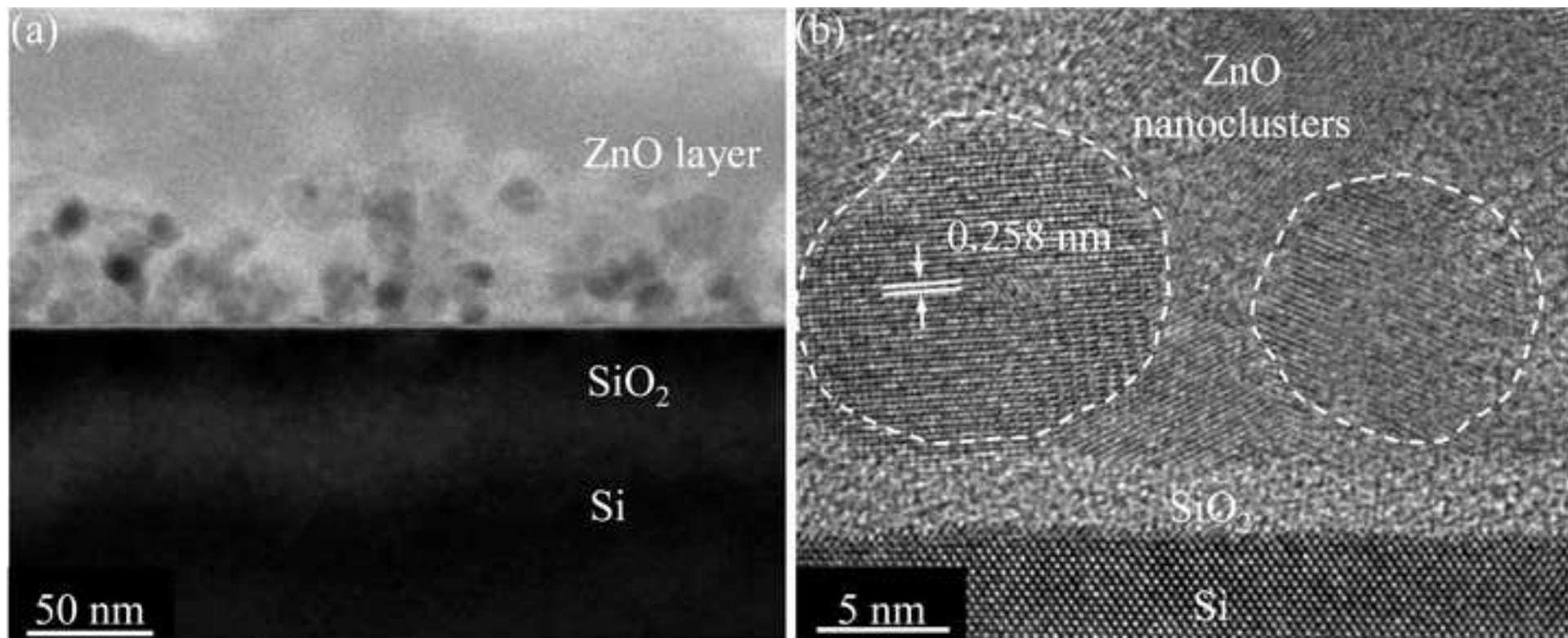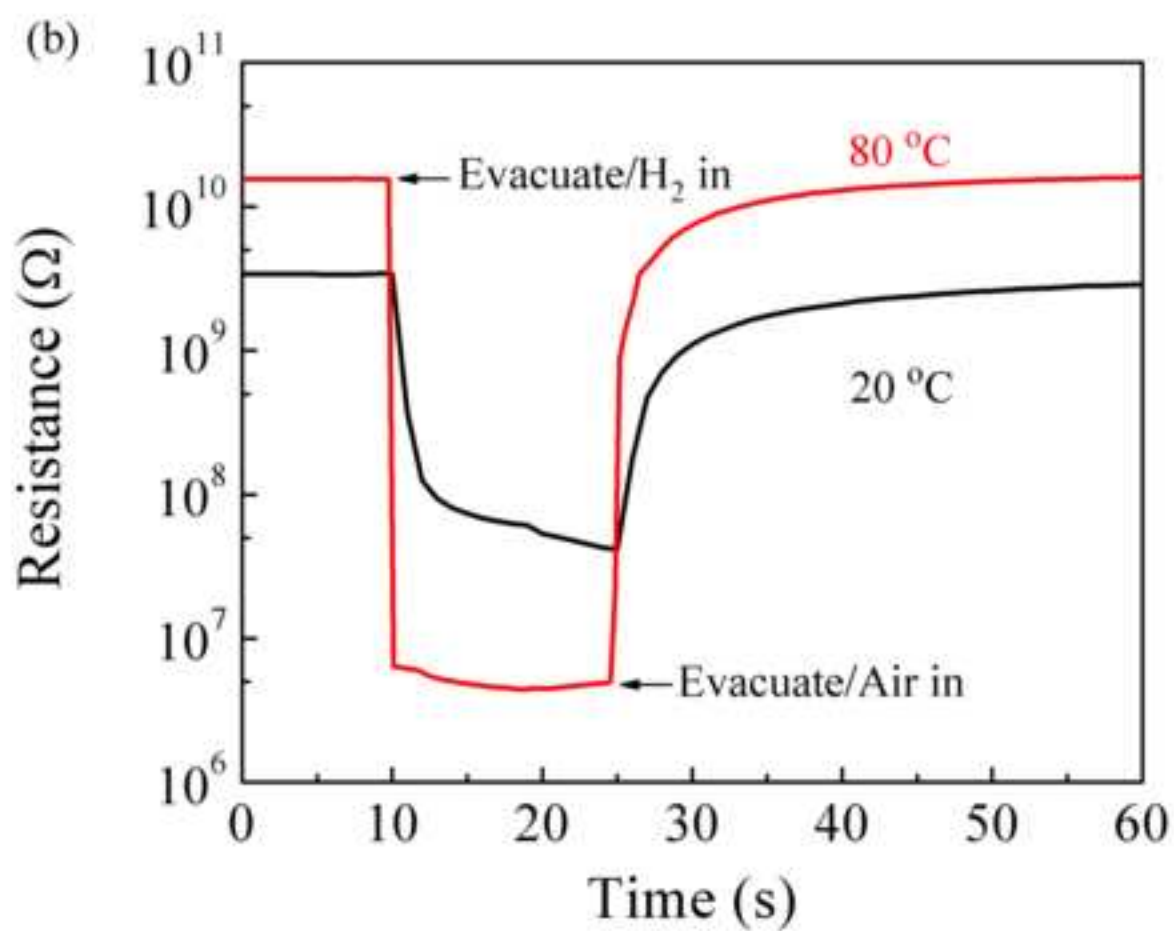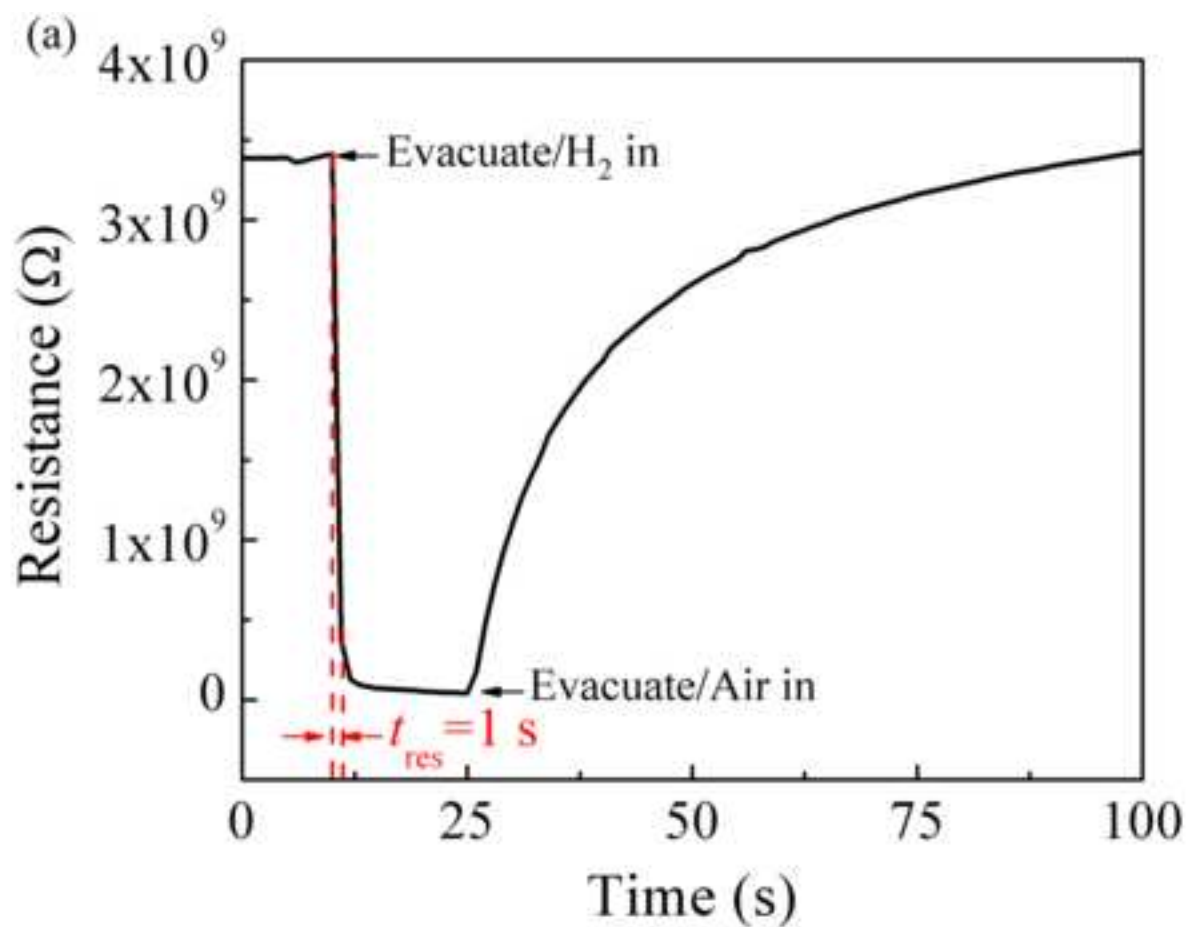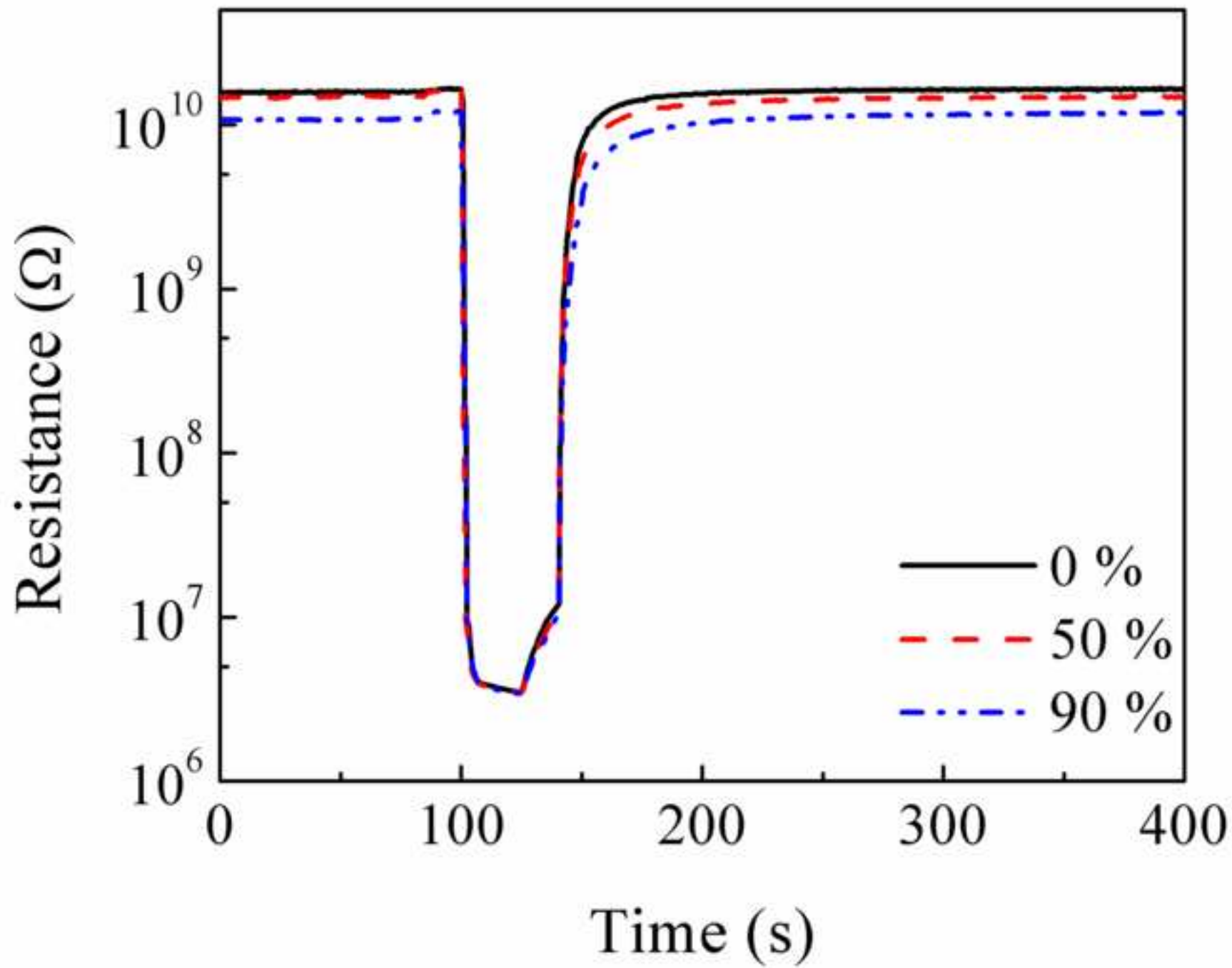
Figure(9)
Click here to download high resolution image

Figure(10)
Click here to download high resolution image

Figure(11)
Click here to download high resolution image